Combined Amino Acid Pet-Mri for Differentiating Recurrence from Radiation Necrosis in Gliomas- Together We Grow

Shumyla Jabeen
Sher-i-Kashmir Institute of Medical Sciences https://orcid.org/0000-0002-3816-4313
Arpana Arbind
National Institute of Mental Health and Neuro Sciences
Dinesh Kumar
National Institute of Mental Health and Neuro Sciences
Pardeep kumar Singh
National Institute of Mental Health and Neuro Sciences
Jitender Saini
National Institute of Mental Health and Neuro Sciences
Nishanth Sadashiva
National Institute of Mental Health and Neuro Sciences
Arivazhagan Arimappamagan
National Institute of Mental Health and Neuro Sciences
Vani Santosh
National Institute of Mental Health and Neuro Sciences
Chandana Nagaraj (dr.chandana@outlook.com)
National Institute of Mental Health and Neurosciences https://orcid.org/0000-0002-8666-8014

Original article

Keywords: Amino acid PET, gliomas, radiation necrosis, recurrence, perfusion, diffusion

Posted Date: March 17th, 2021

DOI: https://doi.org/10.21203/rs.3.rs-301027/v1

Version of Record: A version of this preprint was published at European Journal of Hybrid Imaging on August 18th, 2021. See the published version at https://doi.org/10.1186/s41824-021-00109-y.

Abstract

PURPOSE: To compare the diagnostic accuracy of amino acid PET, MR perfusion and diffusion as stand-alone modalities and in combination in differentiating recurrence from radiation necrosis in post-treatment gliomas and to qualitatively assess spatial concordance between the three modalities using simultaneous PET-MR acquisition.

METHODS: A retrospective review of 48 cases of post-treatment gliomas who underwent simultaneous PET-MRI using C11 Methionine as radiotracer was performed. MR perfusion and diffusion sequences were acquired during the PET study. The following parameters were obtained: TBR_{max}, TBR_{mean}, SUV_{max} and SUV_{mean} from the PET images, rCBV from perfusion, ADC_{mean} and ADC_{ratio} from the diffusion images. The final diagnosis was based on clinical/imaging follow-up and histopathology when available. ROC curve analysis in combination with logistic regression analysis was used to compare the diagnostic performance. Spatial concordance between modalities was graded as 0,1 and 2 representing discordance, <50% and >50% concordance respectively.

RESULTS: There were 35 cases of recurrence and 13 cases of radiation necrosis. The highest area under curve(AUC) was obtained for TBR_{max} followed by rCBV and ADC_{ratio}. The AUC increased significantly with a combination of rCBV and TBR_{max}. Amino acid PET showed the highest diagnostic accuracy and maximum agreement with the final diagnosis. There was discordance between ADC and PET in 22.9%, between rCBV and PET in 16.7% and between PET and contrast enhancement in 14.6% cases.

CONCLUSION

Amino acid PET had the highest diagnostic accuracy in differentiating radiation necrosis from recurrence. Combination of PET with MRI further increased the AUC thus improving the diagnostic performance.

Introduction

Gliomas are the most common primary brain neoplasms (1). Maximal safe surgical excision with adjuvant chemoradiotherapy is the mainstay of treatment for high grade gliomas (grade III and IV). However, recurrence rates continue to remain high with poor overall survival despite treatment especially in case of glioblastoma (2,3). This mandates stringent post-treatment clinical and imaging surveillance. Magnetic Resonance Imaging (MRI) is indispensable for assessment of disease burden and response following therapy. Recent literature has brought focus on the various treatment effects in brain due to radiation therapy, chemotherapy and immunotherapy, the imaging features of which can often resemble tumor recurrence. Distinguishing recurrence from treatment related changes as well as identifying recurrence in a background of such changes is extremely challenging and has profound prognostic and therapeutic implications. There is also a need to set out robust criteria for enrollment in clinical trials and evaluation of efficacy of new emerging therapies. Over several years, the consensus Response Assesment in Neuro-Oncology (RANO) criteria based on conventional MRI and clinical assessment have

been used towards achieving this end (4). Although, there are guidelines for ruling out pseudo-progression with these criteria, this requires a waiting period of 3 months following chemoradiotherapy during which a definitive diagnosis cannot be made (4). Besides, recurrent tumor can often co-exist with radiation necrosis (5) and the two cannot be resolved on conventional imaging alone. Advanced magnetic resonance imaging techniques like perfusion, spectroscopy and quantification of diffusion parameters have shown to be useful in detecting progressive disease as highlighted in several earlier studies, however, at the cost of various challenges in interpretation due to overlapping parameters (6–8). Molecular imaging, which reflects the tumoral physiologic milieu, acts as a problem-solving tool complementary to MRI. FDG-PET has an established role in post-treatment imaging of gliomas (9–11). However, increased uptake by inflammatory cells and high background uptake by the normal brain parenchyma can lead to a false diagnosis (11). In this regard, PET imaging with alternate metabolites like C-11 methionine may be advantageous in view of reduced normal parenchymal uptake. Also, discordance between MR perfusion and FDG-PET was demonstrated in an earlier study highlighting the different functional parameters which they reflect (12). Besides, in most of the early studies based on advanced MRI and PET imaging, the two studies were performed at different time points thus adding to the complexity of the results. In this study, we compared the diagnostic accuracies of amino acid PET, MR perfusion and diffusion as standalone modalities and in combination in differentiating true progression from pseudo progression/radiation necrosis in treated gliomas using simultaneous PET-MR acquisition. In addition, a qualitative assessment of spatial concordance between increased metabolic uptake on PET, elevated perfusion on Dynamic Susceptibility Contrast (DSC) MRI and restricted diffusion on diffusion weighted imaging was performed.

Materials And Methods

Type of study:

This single institute retrospective study was carried out at a dedicated tertiary care centre providing neurosurgical and neuro-imaging services for patients with brain tumors. Informed consent was obtained from all subjects prior to imaging.

Subjects:

All cases of histopathologically proven glial tumors who had undergone surgical resection followed by radiotherapy with or without chemotherapy and underwent simultaneous amino acid PET-MRI for suspected recurrence between January’2019 and March’2020 were included in the study. Exclusion criteria included non-glial primary brain tumors, metastatic lesions and standard contraindications for PET and /or MRI like pregnancy, end-stage renal disease and presence of a cardiac pacemaker or MRI incompatible metallic implants.

Imaging technique:

All patients underwent simultaneous amino-acid PET-MR imaging on a 3 Tesla SIEMENS, Biograph mMR scanner (Erlangen, Germany). All patients were fasted 4-6 hours prior to scanning for baseline stable metabolic conditions. On the day of imaging, all patients were injected 360-378 MBq of C11 methionine on the table through IV cannula. Simultaneous acquisition of PET images was performed along with UTE MR attenuation correction sequence (MRAC) along with other standard and advanced MRI sequences for 40 min in LIST MODE. PET images were acquired using the following parameters: 500mm FOV, 400mm anterior-posterior FOV, 1.0 zoom, 3 interactions, 21 subsets, HD PET reconstruction method, and 2.0mm Gaussian filter.

The following MR sequences were obtained during the PET acquisition:3D Fluid Attenuated Inversion Recovery (FLAIR)- TR/TE= 5000/385msec, TI=1800msec, voxel size=1x1x1mm, FOV=256x256; Axial T1 spin echo- TR/TE= 550/15msec, slice thickness-4mm, FOV=230x230; Axial T2 spin echo- TR/TE=5500/92msec, slice thickness-4mm, FOV=230x230; Axial Susceptibility Weighted Imaging (SWI)- TR/TE=27/20msec, flip angle=15degree, slice thickness=2mm, FOV=230x230; Axial Diffusion Weighted Imaging (DWI)- TR/TE=3900/81msec, slice thickness-4mm, FOV=230x230 at b values of 50 and 1000.

DSC perfusion was performed after the administration of gadolinium-based contrast agent in a dose of 0.1-0.15 mmol/kg body weight at a rate of 5-6ml/sec using a dual chamber injector connected to a 16-gauge cannula placed in the antecubital vein followed by 25ml saline chase at the same rate. Echo planar sequence was acquired with parameters as follows TR/TE= 1900/30msec, flip angle=90 degrees, slice thickness=4mm, FOV= 230x230, no. of slices=25. This was followed by acquisition of post-contrast T1 Magnetization Prepared Rapid Gradient-Echo (MPRAGE) sequence with TR/TE= 2200/2.33msec, TI=900msec, flip angle=8 degrees, FOV=256x256, voxel size=1x1x1mm.

Image Analysis:

The PET and MRI scans were analyzed by a nuclear medicine specialist and neuroradiologist respectively.

PET Analysis:

Quantitative ROI analysis: C11 methionine PET images were loaded into SIEMENS SYNGO Via (VB30) workstation. The ROI was drawn semi-automatically using an individually adapted isocontour of the tumour maximum using a standard ROI with a fixed diameter of 1.6 cm centred on the tumour maximum yielding a volume of 2 mL. Similar mirror ROI was placed in the contralateral brain parenchyma to calculate the background /normal brain parenchymal uptake. The values SUV_{max}, and SUV_{mean} were obtained for both tumour and normal brain parenchyma and tabulated. Ratio TBR_{max} and TBR_{mean} (tumour to normal brain/background) were calculated for statistical analysis.

MRI Analysis-

Quantitative ROI analysis: DSC perfusion, diffusion trace images with ADC maps and post-contrast images were loaded into Philips Intellispace Portal version 6.0. Perfusion images were processed using the leakage correction algorithm. The colored CBV maps were co-registered with the post-contrast image and ROI drawn in the area showing maximum contrast enhancement. A mirror ROI was placed in the contralateral normal white matter and the relative CBV ratio obtained. The ADC maps were also co-registered with the post-contrast images and ROI drawn in the same region of maximum contrast enhancement to obtain the mean ADC value. Another ROI was drawn in the contralateral normal white matter and the ADC ratio calculated.

Qualitative grading of diffusion restriction: A qualitative ordinal scale was used to grade the degree of diffusion restriction on ADC maps with grade 1 assigned when the region of interest appeared brighter than the normal white matter, grade 2 when the signal intensity is same as white matter, grade 3- less than white matter and grade 4- avid, unequivocal diffusion restriction.

Qualitative visual assessment for detecting recurrence: A visual analysis of the rCBV maps, ADC maps and post-contrast images was independently performed to assess for the presence of recurrence without quantification.

Spatial concordance between PET, perfusion and diffusion: The colored rCBV map, ADC map and post-contrast image each were independently compared to the PET image and the spatial concordance between the area of uptake, elevated rCBV on perfusion, restricted diffusion on ADC map and enhancement on post-contrast image graded as follows: grade 0- discordance, 1- fair (less than 50%) and 2- moderate (more than 50 %) concordance between area of PET uptake and elevated perfusion on rCBV map/restriction on ADC map/enhancement on post-contrast T1 MPRAGE.

Final diagnosis: The final diagnosis of recurrence versus radiation necrosis was based on histopathology when available and on clinical and /or imaging follow up for cases where it was not. Disease progression clinically or on imaging was classified as recurrence while stable disease was considered as necrosis.

Statistical Analysis:

Quantitative variables were expressed as median or mean with standard deviation. Qualitative variables were expressed as percentages. The PET, perfusion and diffusion parameters between the two groups were compared using the Mann-Whitney U test. Receiver operating characteristic (ROC) curve analysis was used to assess the diagnostic performance of each parameter in detecting recurrence. ROC curve analysis in combination with logistic regression analysis was used to measure the area under curve of various combination of parameters. The degree of agreement between perfusion, diffusion, contrast enhancement, PET and final diagnosis was estimated using the Cohen kappa statistic with values of .01-.20, .21-.40, .41-.60, .61-.80 and .81-1.00 indicating slight, fair, moderate, substantial and perfect agreement. Spatial concordance between rCBV maps, ADC maps, post-contrast MRI and PET was expressed as percentages. All analysis was performed on IBM SPSS version 26. A p value of less than 0.05 was regarded as significant.

Results

Demographics, primary lesion characteristics and final diagnosis:

There were 48 cases of post-treatment glial brain tumors who underwent simultaneous PET-MR imaging during the study period. The mean age at diagnosis was 39.9± 12.5 years with range of 8-71 years and median 39.5 years. There were 30 males and 18 females with a male:female ratio of approximately 1.7:1. The histopathological diagnosis of the primary neoplasm was glioblastoma multiforme in 16, anaplastic oligodendroglioma in 13, anaplastic astrocytoma in 12, anaplastic ependymoma in 2, high grade undifferentiated glial neoplasm in 1, diffuse midline glioma in 1 and diffuse astrocytoma in 3 cases. Overall, there were 27 grade III lesions, 18 grade IV and 3 grade II lesions.

The final diagnosis was considered as recurrence in 35 cases out of which 9 were confirmed on histopathology and 26 had clinical/imaging evidence of progressive disease. Thirteen cases with no clinical/imaging progression and stable disease were classified as radiation necrosis. The median duration of follow-up after imaging was 7 months ranging between 1 and 14 months (mean 7.5±4 months).

Comparison of quantitative PET, perfusion and diffusion parameters between recurrence and radiation necrosis:

The mean value of each parameter is shown in **table 1**. Intergroup comparison using the Mann-Whitney U test showed a significant difference between the two groups for all PET, perfusion and diffusion parameters. SUV_{max}, TBR_{max} and TBR_{mean} reached the highest level of significance (p value<0.001) followed by rCBV (p value=.001).

Diagnostic performance of PET and MRI parameters:

The ROC curves for each parameter are shown in **Figures 1, 2** with values detailed in **table 2.** Among the PET parameters, the highest area under curve (AUC) was obtained for the TBR_{max} followed by SUV_{max}, TBR_{mean} and SUV_{mean} in that order. For MRI, rCBV ratio showed the highest area under curve followed by ADC ratio, qualitative diffusion restriction grade and mean ADC.

The sensitivity, specificity, positive predictive value, negative predictive value and diagnostic accuracy for each parameter using an appropriate threshold value determined from the coordinates of the ROC curve are shown in **table 2.**

A combined ROC curve analysis was performed with rCBV ratio in combination with TBR_{max} and rCBV alongwith TBR_{max} and ADC ratio. The AUC for rCBV+TBR_{max} was higher than that of rCBV alone (0.908 vs 0.823) showing higher diagnostic accuracy which was statistically significant (p =0.034). Adding ADC ratio further increased the AUC to 0.913, however, the difference was not statistically significant **(Figure 3**).

Agreement of PET, MR perfusion and diffusion diagnosis on visual assessment with the final diagnosis:

Using the Cohen kappa statistic, substantial agreement was seen between PET and the final diagnosis (kappa=0.766) with moderate agreement of rCBV maps (0.472) , ADC maps (0.499) and post-contrast images (0.451).

Concordance between PET, MR perfusion and diffusion:

There was discordance between ADC and PET in 11 cases (22.9%), between rCBV and PET in 8 cases (16.7%) and between PET and contrast enhancement in 7 (14.6%) cases (Figure 4). In case of 11 cases with diffusion-PET discordance, PET correctly classified 9 out of 11 cases as recurrence (Figure 5). Out of 8 cases of discordance between perfusion and PET, only one was incorrectly classified as recurrence on PET while in 7 cases of PET-contrast enhancement discordance, one case was misclassified on PET as recurrence. All instances of incorrect classification on PET were a result of false-positive diagnosis in which radiation necrosis was diagnosed as recurrence (Figure 6). Area of PET uptake and elevated perfusion on MRI showed partial (less than 50%) and near complete (more than 50%) concordance in 12.5 and 70.9 % cases respectively. On ADC maps, partial and near complete concordance of area of diffusion restriction with PET uptake was seen in 14.6 and 62.5 % cases respectively. There was 16.7% partial and 68.8% near complete concordance between contrast enhancement and PET uptake.

Discussion

Differentiating recurrence from radiation necrosis in post-treatment gliomas is critical for patient management. The former requires re-exploration and resection of the tumor, while the latter may be managed medically with steroids. Besides radiation necrosis, other treatment related changes like pseudo-progression and pseudo-response add to the diagnostic confusion. Radiation necrosis occurs around 3 to 12 months following radiotherapy and presents as an increase in post-contrast enhancement on conventional MRI (13). Pseudoprogression results from exaggerated response to treatment and is generally seen within 3 months following radiotherapy with or without chemotherapy. Pseudoresponse occurs due to reduced vascularity following treatment with the anti-angiogenic drug bevacizumab resulting in a decrease in enhancement in an otherwise viable tumor (14).

Conventional magnetic resonance imaging, commonly used for post-treatment follow up of gliomas, falters in differentiating recurrence from treatment related changes since both recurrence, early and delayed radiation changes show an increase in enhancement on post-contrast images secondary to disruption of the blood brain barrier (13,15). MR perfusion, diffusion and molecular imaging techniques provide surrogate markers for angiogenesis and cell proliferation which are features of recurrent tumor (16). Several studies have been performed using these techniques in isolation (9,11,15,17) and combination (6-8,12,18) with variable results.

Molecular imaging is a useful adjunct to advanced MRI in differentiating recurrence from radiation necrosis. Most of the PET studies have been performed using 18-Fluoro-Deoxyglucose (FDG) as the

radiotracer. Although some studies reported a low specificity for FDG-PET in detecting recurrence (19,20), a metanalysis by Wang et al (9) revealed diagnostic performance comparable to magnetic resonance spectroscopy (MRS). In this metanalysis comparing FDG-PET, C-11 Methionine PET and MRS, the pooled sensitivity for FDG-PET was the lowest at 70% and the specificity was highest at 88% (9). The heterogeneity in data related to FDG-PET and lower sensitivity may partly be attributed to the uptake of FDG by the normal brain parenchyma which leads to misdiagnosis in some cases (21). In this regard, amino acid tracers such as C-11 Methionine have a distinct advantage in that the background normal parenchymal uptake is much less thus leading to a higher tumor to background ratio and has shown promising results in various studies (22-26). In our study, the highest AUC and highest diagnostic accuracy were obtained for TBR_{max} with a sensitivity slightly less than that of rCBV ratio (81.8 vs 84.8%) and a much higher specificity (92.3 vs 76.9%) using a threshold of 1.23. These results are comparable to those of other studies which have reported sensitivity and specificity ranging between 66-91% and 60-100% respectively for differentiating recurrent lesion from treatment related changes (22-26). A metanalysis (11) revealed pooled sensitivity of 70% and specificity of 93% for detection of recurrence in high grade gliomas using C11-Methionine PET which is comparable to the values obtained in this study. Besides, we also observed that visual analysis of PET images for recurrence showed the highest agreement with the final diagnosis compared to that of MR perfusion and diffusion. This is expected in view of the increased contrast between lesion uptake and brain parenchyma even in lesions located close to the cortex. Our findings are corroborated by another study (25) in which no significant difference was seen between visual and quantitative analysis in differentiating recurrent brain lesions from radiation necrosis on C11-Methionine PET. However, one of the important disadvantages of C11-Methionine is that uptake may also be seen in areas of radiation necrosis leading to a false positive diagnosis (27). In view of uptake by inflammatory cells, it has been reported to show lower diagnostic accuracy compared to other amino acid radiotracers like Fluroethyltyrosine (FET) and Fluoro-Dihydroxyphenylalanine (F-DOPA) (11,25,28). In this cohort, we encountered a false positive diagnosis in 4 out of 48 cases (8.33%) on Methionine PET in which the findings were discordant with MR perfusion and diffusion.

MR Perfusion has an established role in the detection of recurrent disease. Perfusion parameters are markers of neovascularization which characterizes progressive disease. DSC-perfusion is the most common method used and has been studied in greater detail compared to other methods like dynamic contrast enhanced (DCE) perfusion and arterial spin labelling (ASL) (15). Quantitative assessment of perfusion maps especially rCBV and rCBV ratio calculated in relation to the contralateral normal parenchyma have shown good diagnostic yield in several studies (17,18,29). We obtained a sensitivity and specificity of 84.8 and 76.9% using a cut-off value of 1.38 for rCBV ratio to detect recurrence. Our results are comparable to a pooled analysis which showed sensitivity ranging between 82 to 91% and specificity between 77 and 91% for the detection of recurrence using DSC perfusion (15). However, the threshold rCBV ratio shows wide variation among studies ranging between 0.71 and 3.7 (15). This may be due to co-existence of recurrent disease and radiation necrosis (30) and leakage across the blood brain barrier leading to errors in estimation since DSC perfusion works on the premise that the contrast agent is confined to the intravascular compartment (15). We tried to overcome this limitation to some

extent by using a leakage correction algorithm to process the perfusion study. Visual assessment of rCBV maps showed only moderate agreement with the final diagnosis which was much less than that seen with amino acid PET. This may be accounted for by the fact that small areas of elevated perfusion or lesions near the cortex are likely to be overlooked in view of the background normally perfused brain parenchyma unlike PET using amino acid tracers where an area of uptake distinctly stands out from the rest of the normal brain. Thus, while diagnostic accuracy of quantitative PET and perfusion parameters are comparable, visual assessment of amino acid PET does score over rCBV maps in detecting recurrence, however, at a cost of false positive diagnosis in some cases.

High cell density and continued cellular proliferation in recurrent tumor restricts the diffusion of water molecules seen as a reduction in the ADC values. However, diffusion imaging is limited by the heterogeneity of lesions leading to a relatively poor diagnostic performance (21,31). Among the two quantitative diffusion parameters evaluated in this study, mean ADC and ADC ratio, higher AUC was obtained for ADC ratio with a sensitivity and specificity of 78.1 and 69.2% respectively for detecting recurrent tumor with threshold of 1.11. Using the visual grading scale, grades higher than grade 1 were sensitive (84%) for detecting recurrent disease at the cost of very low specificity of 46.2%. The diagnostic accuracy was 73.65% comparable with other studies (12,18). Also, the threshold ADC ratio of 1.11 shows that the ADC in recurrent lesions is nearly the same as that of the normal white matter thus making visual detection of recurrence on diffusion images difficult. Co-existence of areas of necrosis, recurrent tumor, edema and hemorrhage reflects as marked heterogeneity on diffusion images making it difficult to arrive at a specific diagnosis.

Given the different aspects of tumor biology reflected by each of these imaging modalities, it is intuitive that a combination of parameters provide a more comprehensive picture of the lesional and perilesional milieu resulting in better diagnostic performance. This is supported by the findings of our study which showed a significantly higher AUC for a combination of TBR_{max} and rCBV ratio (0.908) compared to rCBV ratio alone (0.823) thus improving diagnostic accuracy. The AUC further increased with the addition of ADC ratio (0.913), however the difference was not statistically significant. Various studies have shown the superiority of combined PET and MRI over either modality alone (12,32-35). Adding TBR_{max} to choline/creatine ratio (Cho/Cr), rCBV ratio and mean ADC led to an increase in the AUC to 0.932 from 0.913 for MRI alone in a study by Jena et al (12). The best diagnostic performance was seen with a combination of TBR_{mean}, mean ADC and Cho/Cr (AUC=.935). Our results are concordant with a recent study on C11-Methionine PET with DSC perfusion where they obtained an AUC of 0.953 by combining TBR_{max} with rCBV (35). With the advent of hybrid PET-MRI scanners, combined use of structural and functional MRI with metabolic imaging is emerging as an attractive paradigm for evaluation of post-treatment gliomas. It allows simultaneous or sequential acquisition in a single sitting thus reducing time, overcoming logistic hurdles and improving patient convenience and cooperation. Simultaneous acquisition in the same time frame allows better correlation between the dynamics of various functional parameters like uptake on PET and perfusion on MRI. With combined imaging there are less chances of a false negative diagnosis. As was seen in our study, in cases with discordance between PET and perfusion

and/or diffusion on visual analysis, there was no instance of a false negative diagnosis as all cases with recurrence showed uptake on PET. However, false positive diagnosis of recurrence was made in few cases on PET due to uptake seen in radiation necrosis as well.

Elevated perfusion and lower ADC on MRI showed moderate spatial concordance with PET uptake in 70.9 and 62.5% cases respectively. A one is to one spatial correlation is almost never seen. Discordance rate between DSC perfusion and PET for detection of recurrence in our study was 22.9% which is comparable to the rates reported in earlier studies (36,37). A hybrid PET-MRI study on brain tumors with FET as radiotracer showed poor spatial congruence between PET uptake and elevated perfusion (38). Lack of spatial congruence brings to light the fact that areas of increased metabolic uptake on PET and elevated perfusion on MRI represent different aspects of tumor physiology and that elevated perfusion does not directly translate to hypermetabolism and vice versa. The two may co-exist in some regions with variability in rest of the lesion.

Our study had various limitations. It was a retrospective study from a single center. The sample sizes in the groups of recurrence and radiation necrosis were discrepant. We did not have histopathology for all the cases as biopsy in cases of radiation necrosis raises ethical issues. In addition, surgical decompression may not be considered in all cases of recurrence in view of poor Karnofsky performance score in many patients. Also, tumor segmentation may provide more robust results compared to co-registration alone.

Conclusion

Methionine-PET and DSC perfusion are comparable for detecting recurrence in post-treatment gliomas. Diffusion MRI shows lower diagnostic accuracy in view of lesional heterogeneity. Combined PET-MR imaging with C11-methionine as tracer shows superiority over either modality alone and is a feasible option for post-treatment follow-up of gliomas. PET scores over perfusion as well as diffusion MRI in visually detecting recurrence without quantification. One is to one spatial congruence between the modalities is rarely seen as they reflect different aspects of tumor biology.

Declarations

Funding: No funding was received for conducting this study.

Conflicts of interest/competing interests: The authors have no conflicts of interest to declare that are relevant to the content of this article.

Availability of data and material: The data used in the study can be provided if required on request from the corresponding author.

Code availability: Standard software applications have been used for data analysis and are mentioned in the methodology.

Authors' contributions: The data was analysed and the first draft prepared by Shumyla Jabeen; Arpana Arbind helped with manuscript preparation and investigation; Gopinath R was involved in data analysis; Chandana Nagaraj conceptualized the study, provided data and revised the manuscript; Jitender Saini was involved in conceptualization and supervision of the study; Pardeep Kumar Singh was involved in synthesis of the radionuclide used and quality control; Nishanth Sadashiva and Arivazhagan were involved in the clinical aspects of the study and patient selection; Vani Santosh provide the histopathological diagnosis.

Ethical approval: Ethical approval was waivered in view of being a retrospective study which did not involve any intervention.

Consent to participate: Informed consent was obtained from all patients prior to undergoing PET-MR which included consent for participation in research.

Consent for publication: Informed consent was obtained from all patients prior to undergoing PET-MR which included consent for participation in research and publication.

References

1. Ostrom QT, Gittleman H, Truitt G, Boscia A, Kruchko C, Barnholtz-Sloan JS (2018) CBTRUS statistical report: primary brain and other central nervous system tumors diagnosed in the United States in 2011–2015. Neuro-oncology. Oct 1;20(suppl_4):iv1-86
2. Weathers SP, Gilbert MR. Current challenges in designing GBM trials for immunotherapy. Journal of neuro-oncology. 2015 Jul 1;123(3):331-7
3. Stupp R, Mason WP, Van Den Bent MJ, Weller M, Fisher B, Taphoorn MJ, Belanger K, Brandes AA, Marosi C, Bogdahn U, Curschmann J (2005 Mar) Radiotherapy plus concomitant and adjuvant temozolomide for glioblastoma. New England journal of medicine 10(10):987–996 352(
4. Wen PY, Chang SM, Van den Bent MJ, Vogelbaum MA, Macdonald DR, Lee EQ. Response assessment in neuro-oncology clinical trials. Journal of Clinical Oncology. 2017 Jul 20;35(21):2439
5. Sugahara T, Korogi Y, Tomiguchi S, Shigematsu Y, Ikushima I, Kira T, Liang L, Ushio Y, Takahashi M (2000) Posttherapeutic intraaxial brain tumor: the value of perfusion-sensitive contrast-enhanced MR imaging for differentiating tumor recurrence from nonneoplastic contrast-enhancing tissue. American Journal of Neuroradiology. May 1;21(5):901-9
6. Seeger A, Braun C, Skardelly M, Paulsen F, Schittenhelm J, Ernemann U, Bisdas S (2013) Comparison of three different MR perfusion techniques and MR spectroscopy for multiparametric assessment in distinguishing recurrent high-grade gliomas from stable disease. Academic radiology. Dec 1;20(12):1557-65
7. Keunen O, Taxt T, Grüner R, Lund-Johansen M, Tonn JC, Pavlin T, Bjerkvig R, Niclou SP, Thorsen F. Multimodal imaging of gliomas in the context of evolving cellular and molecular therapies. Advanced drug delivery reviews. 2014 Sep 30;76:98–115

8. Heiss WD, Raab P, Lanfermann H (2011) Multimodality assessment of brain tumors and tumor recurrence. Journal of Nuclear Medicine. Oct 1;52(10):1585 – 600
9. Wang X, Hu X, Xie P, Li W, Li X, Ma L (2015 Jun) Comparison of magnetic resonance spectroscopy and positron emission tomography in detection of tumor recurrence in posttreatment of glioma: A diagnostic meta-analysis. Asia-Pacific Journal of Clinical Oncology 11(2):97–105
10. Nozawa A, Rivandi AH, Kanematsu M, Hoshi H, Piccioni D, Kesari S, Hoh CK (2015 Jun) Glucose-corrected standardized uptake value in the differentiation of high-grade glioma versus post-treatment changes. Nucl Med Commun 36(6):573
11. Nihashi T, Dahabreh IJ, Terasawa T (2013) Diagnostic accuracy of PET for recurrent glioma diagnosis: a meta-analysis. American Journal of Neuroradiology. May 1;34(5):944 – 50
12. Jena A, Taneja S, Jha A, Damesha NK, Negi P, Jadhav GK, Verma SM, Sogani SK (2017) Multiparametric evaluation in differentiating glioma recurrence from treatment-induced necrosis using simultaneous 18F-FDG-PET/MRI: a single-institution retrospective study. American Journal of Neuroradiology. May 1;38(5):899–907
13. Verma N, Cowperthwaite MC, Burnett MG, Markey MK (2013) Differentiating tumor recurrence from treatment necrosis: a review of neuro-oncologic imaging strategies. Neuro-oncology. May 1;15(5):515 – 34
14. Zikou A, Sioka C, Alexiou GA, Fotopoulos A, Voulgaris S, Argyropoulou MI. Radiation necrosis, pseudoprogression, pseudoresponse, and tumor recurrence: imaging challenges for the evaluation of treated gliomas. Contrast media & molecular imaging. 2018 Oct;2018
15. van Dijken BR, van Laar PJ, Smits M, Dankbaar JW, Enting RH, van der Hoorn A (2019 Jan) Perfusion MRI in treatment evaluation of glioblastomas: Clinical relevance of current and future techniques. Journal of Magnetic Resonance Imaging 49(1):11–22
16. Ronca R, Benkheil M, Mitola S, Struyf S, Liekens S (2017 Nov) Tumor angiogenesis revisited: regulators and clinical implications. Medicinal research reviews 37(6):1231–1274
17. Barajas RF Jr, Chang JS, Segal MR, Parsa AT, McDermott MW, Berger MS, Cha S (2009 Nov) Differentiation of recurrent glioblastoma multiforme from radiation necrosis after external beam radiation therapy with dynamic susceptibility-weighted contrast-enhanced perfusion MR imaging. Radiology 253(2):486–496
18. Nael K, Bauer AH, Hormigo A, Lemole M, Germano IM, Puig J, Stea B (2018 Jan) Multiparametric MRI for differentiation of radiation necrosis from recurrent tumor in patients with treated glioblastoma. Am J Roentgenol 210(1):18–23
19. Ricci PE, Karis JP, Heiserman JE, Fram EK, Bice AN, Drayer BP (1998) Differentiating recurrent tumor from radiation necrosis: time for re-evaluation of positron emission tomography?. American Journal of Neuroradiology. Mar 1;19(3):407 – 13
20. Hustinx R, Pourdehnad M, Kaschten B, Alavi A (2005 Jan) PET imaging for differentiating recurrent brain tumor from radiation necrosis. Radiologic Clinics 43(1)(1):35–47

21. Soni N, Ora M, Mohindra N, Menda Y, Bathla G (2020) Diagnostic Performance of PET and Perfusion-Weighted Imaging in Differentiating Tumor Recurrence or Progression from Radiation Necrosis in Posttreatment Gliomas: A Review of Literature. American Journal of Neuroradiology. Sep 1;41(9):1550-7
22. Takenaka S, Asano Y, Shinoda J, Nomura Y, Yonezawa S, Miwa K, Yano H, Iwama T (2014 Apr) Comparison of 11C-methionine, 11C-choline, and 18F-fluorodeoxyglucose-positron emission tomography for distinguishing glioma recurrence from radiation necrosis. Neurologia medico-chirurgica 54(4):280
23. Kim YH, Oh SW, Lim YJ, Park CK, Lee SH, Kang KW, Jung HW, Chang KH (2010) Differentiating radiation necrosis from tumor recurrence in high-grade gliomas: assessing the efficacy of 18F-FDG PET, 11C-methionine PET and perfusion MRI. Clinical neurology and neurosurgery. Nov 1;112(9):758–65
24. Deuschl C, Kirchner J, Poeppel TD, Schaarschmidt B, Kebir S, El Hindy N, Hense J, Quick HH, Glas M, Herrmann K, Umutlu L. 11 C–MET PET/MRI for detection of recurrent glioma. European journal of nuclear medicine and molecular imaging (2018) Apr 1;45(4):593–601
25. Minamimoto R, Saginoya T, Kondo C, Tomura N, Ito K, Matsuo Y, Matsunaga S, Shuto T, Akabane A, Miyata Y, Sakai S (2015) Differentiation of brain tumor recurrence from post-radiotherapy necrosis with 11 C-methionine PET: visual assessment versus quantitative assessment. PloS one. Jul 13;10(7):e0132515
26. Terakawa Y, Tsuyuguchi N, Iwai Y, Yamanaka K, Higashiyama S, Takami T, Ohata K. Diagnostic accuracy of 11C-methionine PET for differentiation of recurrent brain tumors from radiation necrosis after radiotherapy. Journal of Nuclear Medicine. 2008 May 1;49(5):694-9
27. Ogawa T, Kanno I, Shishido F, Inugami A, Higano S, Fujita H, Murakami M, Uemura K, Yasui N, Mineura K, Kowada M (1991 May) Clinical value of PET with 18F-fluorodeoxyglucose and L-methyl-11C-methionine for diagnosis of recurrent brain tumor and radiation injury. Acta Radiol 32(3):197–202
28. Galldiks N, Lohmann P, Albert NL, Tonn JC, Langen K-J, Current status of PET imaging in neuro-oncology, *Neuro-Oncology Advances*, Volume 1, Issue 1, May-December 2019,vdz 010
29. Wang S, Martinez-Lage M, Sakai Y, Chawla S, Kim SG, Alonso-Basanta M, Lustig RA, Brem S, Mohan S, Wolf RL, Desai A. Differentiating tumor progression from pseudoprogression in patients with glioblastomas using diffusion tensor imaging and dynamic susceptibility contrast MRI. American Journal of Neuroradiology. 2016 Jan 1;37(1):28–36
30. Blasel S, Zagorcic A, Jurcoane A, Bähr O, Wagner M, Harter PN, Hattingen E (2016 Jan) Perfusion MRI in the evaluation of suspected glioblastoma recurrence. Journal of Neuroimaging 26(1):116–123
31. Brandes AA, Franceschi E, Tosoni A, Blatt V, Pession A, Tallini G, Bertorelle R, Bartolini S, Calbucci F, Andreoli A, Frezza G (2008) MGMT promoter methylation status can predict the incidence and outcome of pseudoprogression after concomitant radiochemotherapy in newly diagnosed glioblastoma patients. Journal of Clinical Oncology. May 1;26(13):2192-7

32. Kim YH, Oh SW, Lim YJ, Park CK, Lee SH, Kang KW, Jung HW, Chang KH (2010) Differentiating radiation necrosis from tumor recurrence in high-grade gliomas: assessing the efficacy of 18F-FDG PET, 11C-methionine PET and perfusion MRI. Clinical neurology and neurosurgery. Nov 1;112(9):758–65
33. Ozsunar Y, Mullins ME, Kwong K, Hochberg FH, Ament C, Schaefer PW, Gonzalez RG, Lev MH (2010) Glioma recurrence versus radiation necrosis?: A pilot comparison of arterial spin-labeled, dynamic susceptibility contrast enhanced MRI, and FDG-PET imaging. Academic radiology. Mar 1;17(3):282 – 90
34. Ozsunar Y, Mullins ME, Kwong K, Hochberg FH, Ament C, Schaefer PW, Gonzalez RG, Lev MH (2010) Glioma recurrence versus radiation necrosis?: A pilot comparison of arterial spin-labeled, dynamic susceptibility contrast enhanced MRI, and FDG-PET imaging. Academic radiology. Mar 1;17(3):282 – 90
35. Qiao Z, Zhao X, Wang K, Zhang Y, Fan D, Yu T, Shen H, Chen Q, Ai L (2019) Utility of dynamic susceptibility contrast perfusion-weighted MR imaging and 11C-methionine PET/CT for differentiation of tumor recurrence from radiation injury in patients with high-grade gliomas. American Journal of Neuroradiology. Feb 1;40(2):253-9
36. Hatzoglou V, Yang TJ, Omuro A, Gavrilovic I, Ulaner G, Rubel J, Schneider T, Woo KM, Zhang Z, Peck KK, Beal K (2016) A prospective trial of dynamic contrast-enhanced MRI perfusion and fluorine-18 FDG PET-CT in differentiating brain tumor progression from radiation injury after cranial irradiation. Neuro-oncology. Jun 1;18(6):873 – 80
37. Seligman L, Kovanlikaya I, Pisapia DJ, Naeger DM, Magge R, Fine HA, Chiang GC (2019 Apr) Integrated PET-MRI for glioma surveillance: perfusion-metabolism discordance rate and association with molecular profiling. Am J Roentgenol 212(4):883–891
38. Filss CP, Galldiks N, Stoffels G, Sabel M, Wittsack HJ, Turowski B, Antoch G, Zhang K, Fink GR, Coenen HH, Shah NJ (2014) Comparison of 18F-FET PET and perfusion-weighted MR imaging: a PET/MR imaging hybrid study in patients with brain tumors. Journal of Nuclear Medicine. Apr 1;55(4):540-5

Tables

Table 1: Median, mean, standard deviation (SD) for PET, perfusion and diffusion parameters in either group with p values obtained using the Mann-Whitney test:

PARAMETERS	RECURRENCE=35 Mean, Median (SD)	RADIATION NECROSIS=13 Mean, Median (SD)	p VALUE
TBR_{max}	1.83,1.59 (1.05)	1.03,1.02 (0.18)	.000
TBR_{mean}	1.67,1.57 (1.01)	0.90,0.95 (0.30)	.000
SUV_{max}	4.72,4.36 (2.15)	2.66,2.64 (0.80)	.000
SUV_{mean}	2.44,2.15 (1.3)	1.52,1.57 (0.70)	.019
$rCBV_{ratio}$	2.94,2.00 (1.8)	0.99,0.67 (0.94)	.001
ADC_{mean}	0.78,0.77 (0.14)	0.99,0.95 (0.38)	.032
ADC_{ratio}	0.99, 0.96 (0.25)	1.49,1.3 (0.73)	.004

TBR= Tissue Background Ratio, SUV- Standard Uptake Value, rCBV- Relative Cerebral Blood Volume, ADC- Apparent Diffusion Co-efficient

Table 2: Area under curve values with sensitivity, specificity, positive predictive values (PPV), negative predictive values (NPV) and diagnostic accuracy for important PET, perfusion and diffusion parameters.

PARAMETER	AUC	CUT-OFF	SENSITIVITY (%)	SPECIFICITY (%)	PPV (%)	NPV (%)	DIAGNOSTIC ACCURACY(%)
TBR_{max}	0.865	1.23	81.8	92.3	91.4	83.5	87.05
$rCBV_{ratio}$	0.823	1.38	84.8	76.9	78.6	83.5	80.85
ADC_{ratio}	0.776	1.11	78.1	69.2	71.7	75.9	73.65
ADC_{grade}	0.722	>1	84	46.2	60.9	74.3	65.1

TBR= Tissue Background Ratio, , rCBV- Relative Cerebral Blood Volume, ADC- Apparent Diffusion Co-efficient

Figures

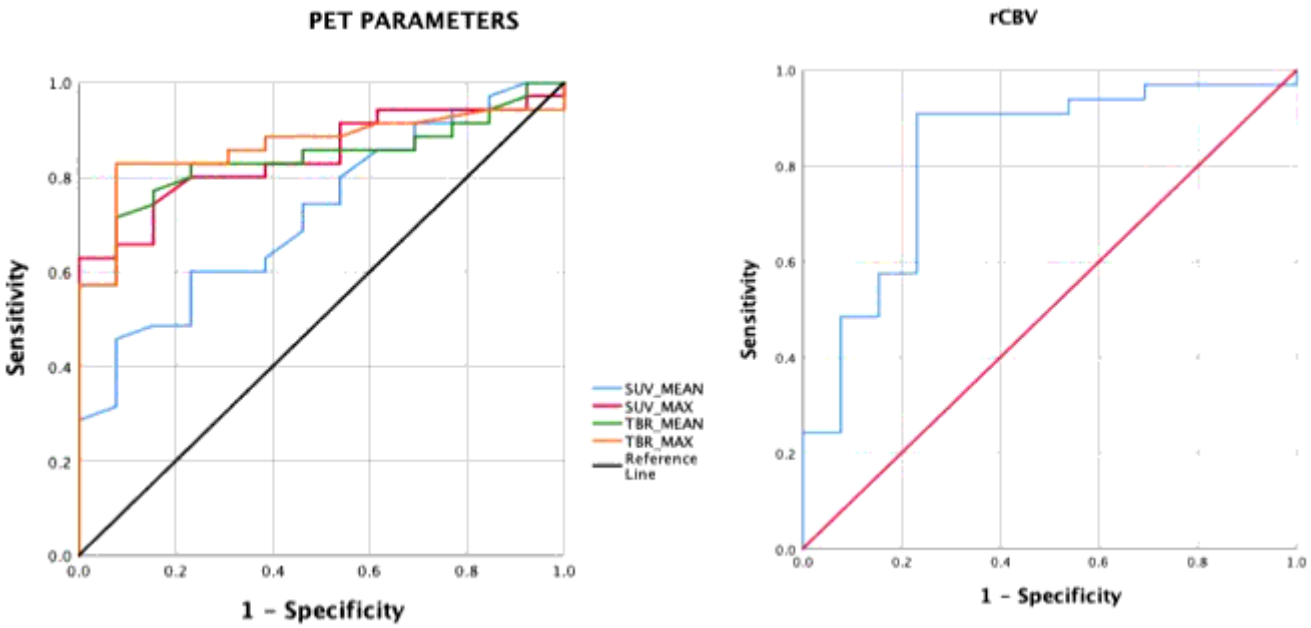

Figure 1

ROC curve analysis for PET parameters on the left and relative CBV on the right. The highest area under curve was obtained for TBRmax among the PET parameters followed by SUVmax, TBRmean and SUVmean in that order.

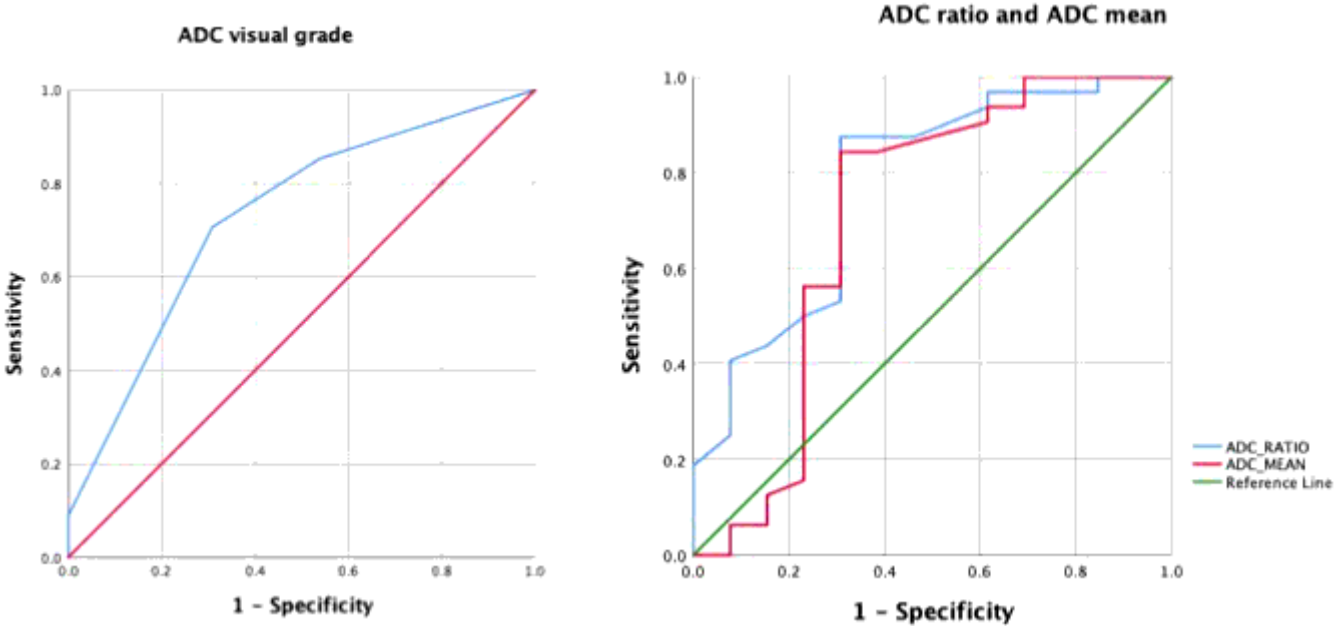

Figure 2

ROC curves for ADC visual grade on the left and ADCratio as well as mean ADC on the right. The lowest area under curve among the diffusion parameters was that for mean ADC.

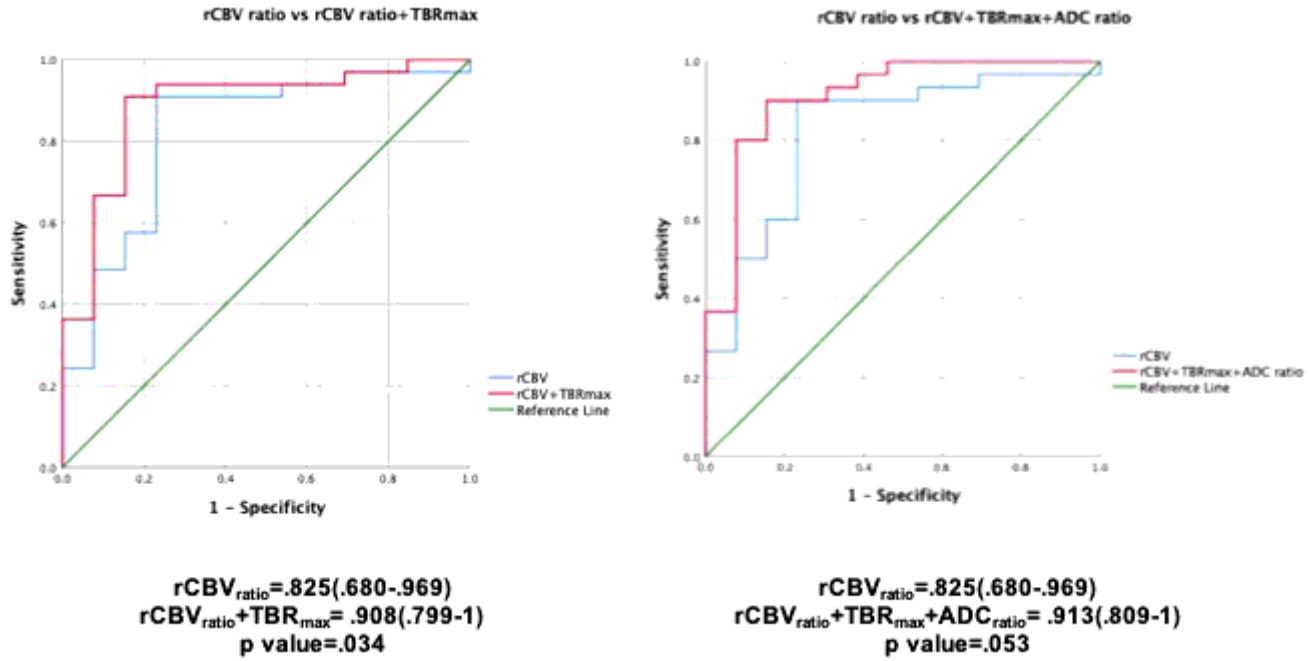

$rCBV_{ratio}$=.825(.680-.969)
$rCBV_{ratio}+TBR_{max}$= .908(.799-1)
p value=.034

$rCBV_{ratio}$=.825(.680-.969)
$rCBV_{ratio}+TBR_{max}+ADC_{ratio}$= .913(.809-1)
p value=.053

Figure 3

ROC curves for relative CBV and TBRmax combined compared to relative CBV alone is shown on the left. The graph on the right shows the ROC curve for relative CBV with TBRmax and ADCratio compared to relative CBV alone. The area under curve for rCBV and TBRmax taken together increased to 0.908 compared to 0.825 for rCBV alone with statistically significant difference. The area further increased to 0.913 with ADCratio without reaching statistical significance.

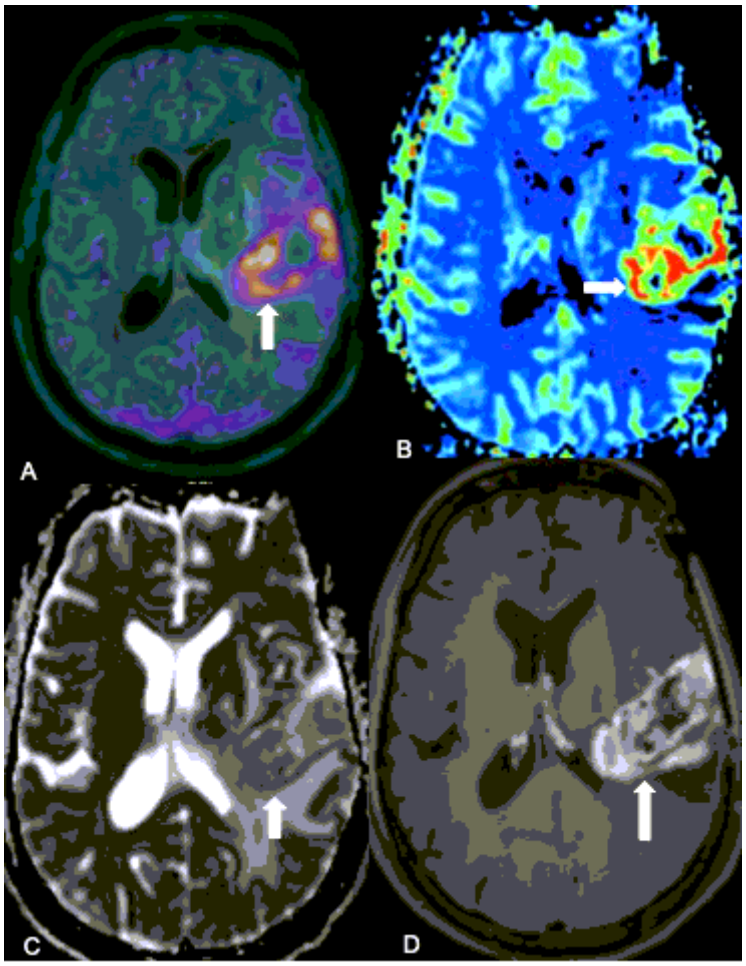

Figure 4

Concordant PET, perfusion, diffusion and enhancement in a case of recurrence: 40 year old male diagnosed with anaplastic ODG 15 months back with recurrence- HPE showed wild-type GBM in recurrent lesion. Radiotherapy completed 12 months earlier. PET image overlaid over T1 MPRAGE (A) shows a large area of uptake in the left temporoparietal region (white arrow). rCBV map (B) generated with the leakage correction algorithm shows elevated perfusion in the same region (white arrow) with diffusion restriction on the ADC map (white arrow in C). Note enhancement on the post-contrast image (white arrow in D). This is a case of recurrence where the PET, perfusion, diffusion and contrast images were concordant with good spatial congruence.

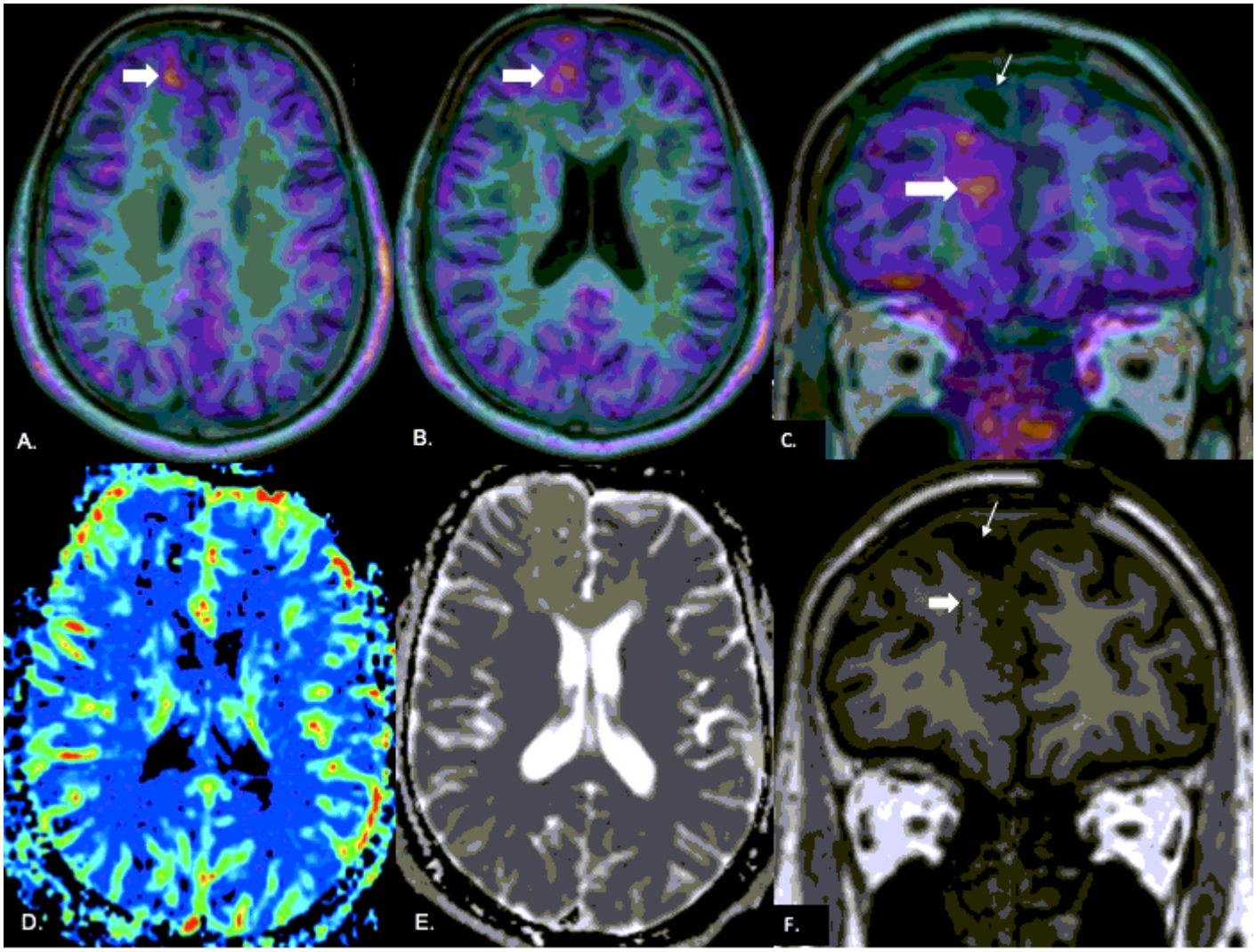

Figure 5

Discordance between PET, perfusion and diffusion in a case of recurrence: 31 year old male operated for right frontal ODG 14 months back; last radiation dose 10 months ago. PET images fused with axial T1 MPRAGE (A,B) show an area of uptake in the right superior frontal gyrus (white arrow in A,B). The uptake (block white arrow) is seen along the margins of the resection cavity (small white arrow) on the coronal fused PET-MR image (C). rCBV map (D) generated using the leakage correction algorithm shows no unequivocal elevation of perfusion in the area. There is no diffusion restriction on the ADC map (E). A small focus of enhancement (block white arrow) is seen along the margins of the resection cavity (small white arrow) on post-contrast coronal T1 MPRAGE (F).

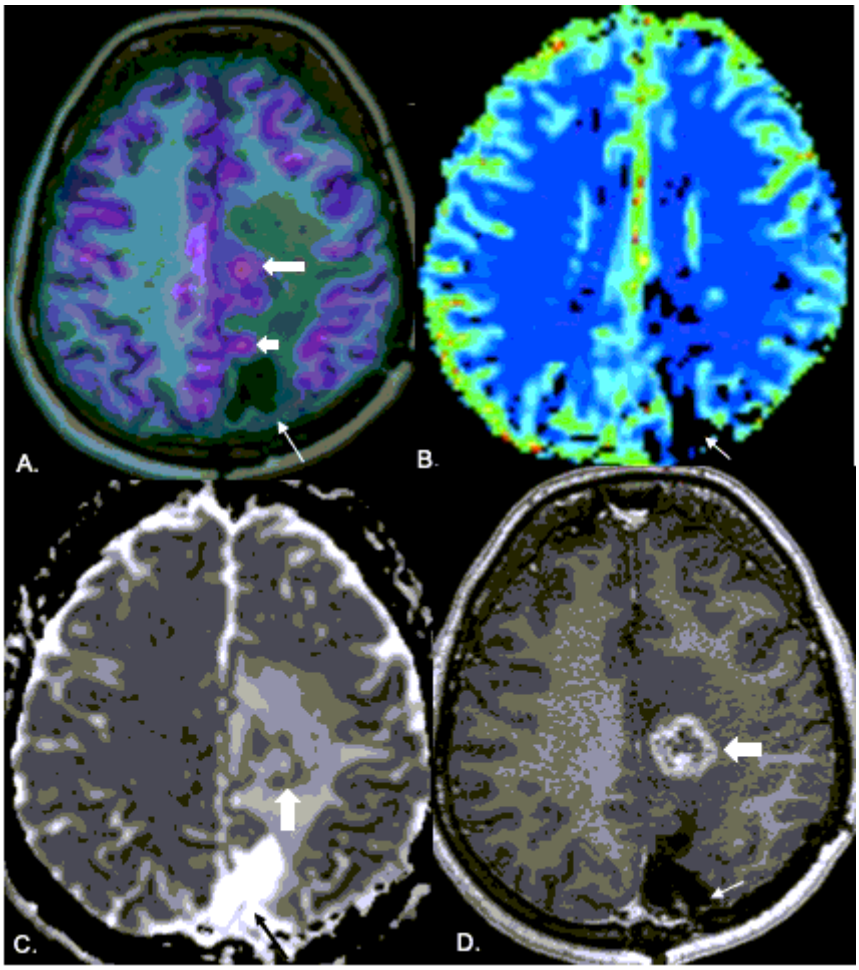

Figure 6

False positive diagnosis on PET: 34 year old female diagnosed with anaplastic ODG 2 years back with enhancing lesion on MRI. PET image fused with axial T1 MPRAGE (A) shows an area of uptake along the parasagittal region of the left frontal lobe (large thick arrow) and another area (small thick arrow) along the margin of the resection cavity (linear white arrow) raising a suspicion of recurrence. There is no evidence of elevated perfusion on the rCBV map (B). Resection cavity is shown by white arrow. Peripheral diffusion restriction is seen along the margins of the lesion in the left centrum semiovale (block white arrow in C). There is no restriction along the resection cavity (black arrow). Peripheral enhancement is seen along the margins of the lesion in the left centrum semiovale (block white arrow in D) with no enhancement along the resection cavity (white arrow). The patient had stable disease and continues to be on follow-up.